IEEE Access
Multidisciplinary | Rapid Review | Open Access Journal

Received July 17, 2019, accepted September 3, 2019, date of publication September 16, 2019,
date of current version September 27, 2019.

Digital Object Identifier 10.1109/ACCESS.2019.2941591

Real-Time Simulation of a Rescue Ship Maneuvering in Short-Crested Irregular Waves

XIAOLEI ZHANG[1], WEI XIONG[1], XU XIANG[2], AND ZUWEN WANG[1]
[1]Institute of Ship Electromechanical Equipment, Dalian Maritime University, Dalian 116026, China
[2]Norwegian Public Roads Administration, 0667 Oslo, Norway

Corresponding author: Wei Xiong (xiongwei@dlmu.edu.cn)

This work was supported by the Fundamental Research Funds for the Central Universities of China under Grant 3132018210.

ABSTRACT Research on the mathematical model and the real-time simulation of the ship motion is investigated. An equation of three degrees of freedom (DOF) nonlinear maneuvering motion is established by means of the unified model in short-crested irregular waves in deep water. The resistance and propulsion dynamics are modeled by the classical methods as well as forces and moments of the rudder and the viscous crossflow. The three-dimensional boundary element method (BEM) using Green function source is adopted to solve the boundary value problem (BVP) in the frequency domain. The added mass and potential damping coefficients are calculated by Cummins method, and the mean wave drift forces by far-field formulas along with numerical verifications. After that, the turning motions of two ships (a rescue ship NHJ111 and the Mariner) in calm water are performed, and the relative error is approximately 7% by comparing calculated results with the experimental data. The maneuvering motion of the Mariner in short-crested irregular waves is then carried out. The turning trajectory, surge speed, and drift forces agree well with the theoretical results in regular waves. Finally, the synchronous interpolation method with two-thread double-timer is conceived. The real-time maneuvering simulation of NHJ111 using the validated model is then realized. The developed method can lay the foundation for fast computations of predicting the rescue ship motions in waves.

INDEX TERMS Mean wave drift forces, rescue ship maneuverability, real-time simulation, short-crested irregular waves.

I. INTRODUCTION

When maritime accidents occur, rescue ships are usually employed to save human lives, properties, the environment, and ships [1], [2]. Equipped with rescue devices, stabilizers, and auxiliary thrusters, a rescue ship has the characteristics of strong towing ability and good maneuverability, which make the ship capable of resisting the influences of environmental disturbances. Therefore, rescue ships serve as one of the most effective ways to implement rescue operations in extreme sea conditions. As an important part of the rescue process, rescuers should take appropriate actions at the crucial moment, which have a significant impact on the success of a rescue operation. Training for emergency operations with a rescue ship simulator has the advantages of high safety, low cost, short cycle, and great efficiency compared to training with real ships. One of the key technologies for the rescue ship simulator is the mathematical model of ship motions. Consequently, it is necessary to develop a high accuracy model used in the rescue ship simulator for real-time calculations.

The maneuverability of a ship is usually analyzed in calm water. There are some types of mathematical models established using different methods, including the integrated models in which Taylor expansions are used to express hydrodynamic loads of the hull; the models of Maneuvering Model Group (MMG) in which the hull, propeller, and rudder are modeled separately and interactions between them are considered; responsive models of single-input single-output (SISO); and the black-box or gray-box models based on system identification algorithms [3]–[5].

When considering a ship moving in waves, it is necessary to combine the maneuvering and seakeeping to establish a unified mathematical model. There are two distinctive methods [6]: the two-time scale model and the integro-differential model based on the Cummins equation. The two-time scale model [7]–[9] divides the motions into high-frequency wave-induced motions and low-frequency maneuvering motions. The former is frequency dependent, and the latter one can be assumed as zero-frequency motions.

The associate editor coordinating the review of this manuscript and approving it for publication was Zheng H. Zhu.

The MMG model can be used to construct a two-time scale model. Then, the maneuvering and seakeeping problems are analyzed separately with related data exchanged. The other modeling method, namely, the integro-differential model based on the Cummins equation [10]–[12], uses Fourier transform and its inverse transform to effectively convert the radiation forces in the frequency domain into those in the time domain in the form of a convolution integral. The above two unified models can be both based on the modular concept, where the hydrodynamic loads of the hull, rudder, propeller, and wave effects as well as the resistance in calm water are modeled in different modules.

When a ship moves in waves, the second-order wave forces are small in the low-frequency and high-frequency parts compared to the forces with the incident wave frequency. The latter can be ignored since it causes the hull to generate structural vibration but does not affect the ship motions. The mean second-order wave forces at steady state cannot be ignored since it causes the ship drift and the speed drop [7], [8].

In order to improve the accuracy of the mathematical model in the ship simulator, it is necessary to consider the second-order drift forces. Zhang *et al.* [13] proposed a simplified three degrees of freedom (DOF) responsive model used in a ship simulator with multiple ships for fast simulations. The wave spectrum driven by white noise was used to simulate the first-order wave-induced motions. However, the accuracy was low and the effects of the second-order wave drift forces were not considered. Zhang [14] developed a 6DOF mathematical model for a ship simulator based on the MMG model, and the first-order wave forces were estimated both in regular and irregular waves, and the second-order drift forces were not considered. In this method, the hull was approximated as a box-shape body, and the Froude-Kriloff hypothesis was employed that only considers the effects of the incident wave field. Accordingly, the performance of real-time calculations was guaranteed by sacrificing the accuracy of the model.

Later on, Zhang *et al.* [15] also developed a 3DOF nonlinear model for a small-waterplane-area twin-hull (SWATH) in the ship simulator. In this model, the hydrodynamic loads of the hull, propeller, and rudder were estimated by using empirical formulas. However, wave forces were not included and the ship motions were only qualitatively analyzed. Qian *et al.* [16] developed a 6DOF model for a ship dynamic positioning simulator. The modeling methods of the first-order wave forces were similar to those proposed by Zhang *et al.* [15]. The second-order drift forces were calculated by using estimating formulas. However, the predictions of ship motions under the action of wave forces were not directly given. Fang *et al.* [17] proposed a 4DOF MMG model used by a PC-based ship simulator. In the method, horizontal motions were decoupled from the rolling motion. The hydrodynamic coefficients were estimated by using empirical formulas, and the wave-induced motions were calculated by using the 2D strip method. A motion database of different ship speeds in regular waves was thus established for real-time interpolations. However, the drift forces were not considered, either.

Additionally, Ueng *et al.* [18] and Damitha *et al.* [19] developed a simulation system of ship motions for educational applications, in which a responsive model was employed. First-order wave-induced motions were described using a corrected wave field height at the waterline of the ship, and the requirements for real-time calculations were achieved without considering the dynamic characteristics of the free surface. Chen *et al.* [20] proposed a mathematical model of ship motions in waves for real-time calculations, in which the incident waves were decomposed into a linear combination of head waves and transverse waves. Therefore, the ship motions was simulated by combining the oscillations caused by the decomposed transverse waves and head waves. Pinkster and Bhawsinka [21] used a modular type maneuvering model in the real-time maneuvering simulator at MARIN, and created the databases of ship-ship interaction forces for interpolations by using a hydrodynamic software Delpass, which was based on the double-body potential flow theory. However, they did not take into account the influence of the wave forces on the ship motions. The above methods simplified the modeling of wave forces for the purpose of real-time calculations.

Mean second-order wave drift forces can be described by four commonly used methods. The first one is the near-field formulation based on the direct pressure integral method [22], which can calculate all the six components of drift loads. However, the convergence rate for numerical calculations is relatively slow. In addition, numerical integrals are not possible at sharp corners. The second one is the mid-field formulation based on applying Stokes' theorem and Guass's theorem directly to the near-field formulation [23], resulting to a formulation expressed on a control surface around the hull with a finite distance. An alternative to the mid-field method is by applying the conservation of momentum on the control surface. The convergence rate of the mid-field method is fast. The third one is the far-field formulation based on the conservation of momentum [24], which can calculate the drift loads including surge forces, sway forces, and yaw moments. The method has the advantage of being robust with fast convergence for numerical calculations. The last one is known as the short-wavelength asymptotic theory [22], which is applicable to scenarios where the ratio of the wavelength over the ship length is $\lambda/L <\approx 0.5$, the Froude number is $F_n <\approx 0.2$ and block coefficient is $C_b > 0.75$.

Zhang *et al.* [25] developed a 3DOF mathematical model based on the two-time scale modeling concept in regular waves. In this model, the base flow potential was evaluated by using the double-body method with a trailing vortex sheet, whereas the perturbation potential was solved via a time domain Rankine panel method. Then the pressure integral method was used to calculate the second-order wave drift loads. The influence of the maneuvering motions on the wave forces was considered through the m-terms. The above model was used to simulate and verify the turning and zig-zag maneuvers of the S175 container ship, resulting in good

agreements compared with the experimental data. Yasukawa and Nakayama [26] established a 6DOF two-time scale model in regular waves under the quasi-steady assumption of ignoring the fluid memory effects, which is generated by the wave-making radiation. The second-order drift forces were calculated by using the far-field method.

Furthermore, Seo and Kim [27] conducted the simulations of the turning motions of the Series60 and S175 ships in regular waves by using a 4DOF two-time scale model. The velocity potential was calculated by the Rankine source method, and the mean second-order drift forces were evaluated by the direct pressure integration method. It was shown that the numerical results were in good agreement with experimental data in calm water. However, when the mean second-order drift forces were considered, there were some discrepancies between the calculated trajectory and the experimental data. A similar study was performed by Lee and Kim [28]. Chillcce and Moctar [29] developed a 6DOF mathematical model with hull forces and rudder forces represented by Taylor expansions, and the hydrodynamic derivatives estimated by the Reynolds Averaged Navier-Stokes (RANS) method. Mean drift forces were calculated by the near-field method based on the Rankine source method. Comparisons with the experimental data showed that the mathematical model still needed improvement.

Generally, the above methods all consider the modeling of drift forces from a theoretical point of view. However, the corresponding calculations are time-consuming.

The mathematical model used in the ship simulators is supposed to have high-precision and good performance for real-time calculations. Most of the aforementioned models utilized in ship simulators are simplified to achieve real-time calculations, especially the wave load models.

Taking the accuracy and real-time requirements into account, this paper presents a mathematical model together with the mean drift forces calculated in short-crested irregular waves. The 3DOF nonlinear maneuvering equations are established by using the maneuvering and seakeeping unified model. The Green function method is applied to solve the velocity potential, and the drift forces are evaluated by the far-field method with the numerical verification in the frequency domain. The turning maneuvers of a rescue ship NHJ111 and the Mariner are conducted both in calm water and in short-crested irregular waves in deep water. The comparisons of results between this study and others are performed to verify the models. Then the programming design for real-time calculations are conceived by a two-thread double-timer interpolation method, and the visual simulation of NHJ111 motions subjected to the drift forces in short-crested irregular waves is implemented.

II. MATHEMATICAL MODELS

A. KINEMATIC TRANSFORMATIONS

The kinematics and dynamics of a ship can be analyzed by using multiple coordinate systems depending on the purposes of study. When analyzing the maneuverability of a ship in waves, two Cartesian coordinate systems are employed [12], i.e. the maneuvering coordinate system and the seakeeping coordinate system, as shown in Figure 1.

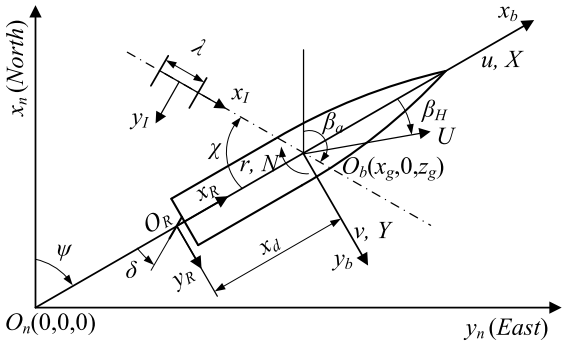

FIGURE 1. Definition of Coordinate systems.

The maneuvering coordinate system includes a body-fixed reference frame O_b-$x_by_bz_b$ and an earth-fixed reference frame O_n-$x_ny_nz_n$. The equations of the ship motions are established in O_b-$x_by_bz_b$ with x_b pointing to the bow, y_b pointing starboard, z_b pointing to the keel, and O_b located at the center of gravity $\boldsymbol{r}_{\boldsymbol{g}}^{\boldsymbol{b}} = [x_g y_g z_g]^T$. The ship global positions are described in O_n-$x_ny_nz_n$ with x_n pointing to true North, y_n pointing to East, z_n pointing downwards normal to the earth's surface, and O_n located on the surface of the calm water. The seakeeping coordinate system O_s-$x_sy_sz_s$ coincides with O_b-$x_by_bz_b$ in the initial equilibrium state and moves with the ship speed U.

The velocities expressed in O_b-$x_by_bz_b$ can be transformed to O_n-$x_ny_nz_n$ according to

$$\dot{\boldsymbol{\eta}} = \boldsymbol{J}(\boldsymbol{\eta})\boldsymbol{\nu}, \tag{1}$$

where $\boldsymbol{\eta} = [x\ y\ \psi]^T$ is the vector representing the positions and Euler angle in horizontal plane, $\boldsymbol{\nu} = [u\ v\ r]^T$ contains the velocities in O_b-$x_by_bz_b$, and $\boldsymbol{J}(\eta)$ is the transformation matrix, expressed as

$$\mathbf{J}(\boldsymbol{\eta}) = \begin{bmatrix} \cos\psi & -\sin\psi & 0 \\ \sin\psi & \cos\psi & 0 \\ 0 & 0 & 1 \end{bmatrix}, \tag{2}$$

where the heading angle $\psi \in [0, 2\pi)$.

The propagation of an incident wave is represented in the reference frame O_I-$x_Iy_Iz_I$ with x_I pointing to the wave propagation direction and z_I pointing downwards. β_a is the wave angle relative to O_n-$x_ny_nz_n$. The encounter wave angle can be expressed as $\chi = \beta_a - \psi$, as shown in Figure 1, $\chi = 0°$ and $\chi = 180°$ mean following sea and head sea, respectively. The axial directions of the above coordinate systems follow the right-handed rules.

B. MATHEMATICAL MOTION EQUATIONS

The mathematical equations of ship motions are expressed by using a modular approach. The following assumptions are made: the hull is rigid and symmetrical about the plane $x_bO_bz_b$; only the mean second-order wave drift forces are

considered for external disturbances; and the motions of heave, pitch, and roll are neglected, i.e. only ship motions in the horizontal plane are considered. In the reference frame O_b-$x_by_bz_b$, the 3DOF nonlinear unified mathematical model in the time domain is expressed as the following matrix form using Cummins equation [10], [12]

$$[\boldsymbol{M_{RB}} + \boldsymbol{M_A}(\infty)]\dot{\boldsymbol{v}} + [\boldsymbol{C_{RB}}(\boldsymbol{v}) + \boldsymbol{C_A}(\boldsymbol{v})]\boldsymbol{v} + [\boldsymbol{D}(\infty) + \boldsymbol{D_n}(\boldsymbol{v})]\boldsymbol{v} + \boldsymbol{\mu} + \boldsymbol{g}(\boldsymbol{\eta}) = \boldsymbol{\tau} + \boldsymbol{\tau_{wave2}}, \quad (3)$$

where

$$\boldsymbol{\mu} = \int_0^t \mathbf{h}(t-\tau)\delta\mathbf{v}(\tau)d\tau, \quad (4)$$

is a damping force known as the fluid memory effects for the radiation waves generated by ship motions in the free surface. The quantity is the result from the added mass and potential damping converted from the frequency domain to the time domain by using the convolution of the impulse response function $\boldsymbol{h}(t)$ and the perturbation velocity $\delta\boldsymbol{v}(t)$. The quantity μ and the hydrostatic vector $\boldsymbol{g}(\ \eta)$ are ignored since we only consider motions in the horizontal plane. The hydrodynamic coefficients are frequency independent and can be approximated as constants. Therefore, (3) is simplified as

$$[\boldsymbol{M_{RB}} + \boldsymbol{M_A}(\infty)]\dot{\boldsymbol{v}} + [\boldsymbol{C_{RB}}(\boldsymbol{v}) + \boldsymbol{C_A}(\boldsymbol{v})]\boldsymbol{v} + [\boldsymbol{D}(\infty) + \boldsymbol{D_n}(\boldsymbol{v})]\boldsymbol{v} = \boldsymbol{\tau_R} + \boldsymbol{\tau_P} + \boldsymbol{\tau_{wave2}}, \quad (5)$$

where $\boldsymbol{M_{RB}}$ is the rigid-body inertia matrix, $\boldsymbol{M_A}(\infty)$ and $\boldsymbol{D}(\infty)$ are the constant infinite-frequency matrices of added mass and potential damping, respectively, $\boldsymbol{C_{RB}}(\boldsymbol{v})$ and $\boldsymbol{C_A}(\boldsymbol{v})$ are the Coriolis-centripetal matrices of ship hull and added mass, respectively, $\boldsymbol{D_n}(\boldsymbol{v})$ is the nonlinear viscous damping matrix, $\tau_{\mathbf{R}}$ and $\tau_{\mathbf{P}}$ are the forces and moments of the rudder and propeller, respectively, and $\boldsymbol{\tau_{wave2}}$ contains the mean wave drift forces and moments. They are given by

$$\boldsymbol{M_{RB}} = \begin{bmatrix} m & 0 & 0 \\ 0 & m & mx_g \\ 0 & mx_g & I_z \end{bmatrix}, \quad (6)$$

$$\boldsymbol{M_A}(\infty) = -\begin{bmatrix} X_{\dot{u}} & 0 & 0 \\ 0 & Y_{\dot{v}} & Y_{\dot{r}} \\ 0 & N_{\dot{v}} & N_{\dot{r}} \end{bmatrix}, \quad (7)$$

$$\boldsymbol{C_{RB}}(\boldsymbol{v}) = \begin{bmatrix} 0 & -mr & -mx_gr \\ mr & 0 & 0 \\ mx_gr & 0 & 0 \end{bmatrix}, \quad (8)$$

$$\boldsymbol{C_A}(\boldsymbol{v}) = \begin{bmatrix} 0 & 0 & Y_{\dot{v}}v + Y_{\dot{r}}r \\ 0 & 0 & -X_{\dot{u}}u \\ -Y_{\dot{v}}v - Y_{\dot{r}}r & X_{\dot{u}}u & 0 \end{bmatrix}, \quad (9)$$

$$\boldsymbol{D}(\infty) = -\begin{bmatrix} 0 & 0 & 0 \\ 0 & Y_v & Y_r \\ 0 & N_v & N_r \end{bmatrix}, \quad (10)$$

$$\boldsymbol{D_n}(\boldsymbol{v})\boldsymbol{v} = -\begin{bmatrix} 0 \\ Y_{CF} \\ N_{CF} \end{bmatrix}, \quad (11)$$

$$\boldsymbol{\tau_R} = \begin{bmatrix} X_R & Y_R & N_R \end{bmatrix}^T, \quad (12)$$

$$\boldsymbol{\tau_P} = \begin{bmatrix} -R(u) + X_P & 0 & N_P \end{bmatrix}^T, \quad (13)$$

$$\boldsymbol{\tau_{wave2}} = \begin{bmatrix} \overline{R_X} & \overline{R_Y} & \overline{M_Z} \end{bmatrix}^{\boldsymbol{T}}, \quad (14)$$

where m is the rigid body mass, x_g is the longitudinal coordinate of the gravity center in O_b-$x_by_bz_b$, and I_z is the inertia moment along the z_b axis. X_R, Y_R, and N_R are the rudder forces and moment, respectively. For a twin-rudder ship, we have

$$\begin{cases} X_R = F_{Rxp} + F_{Rxs} \\ Y_R = F_{Ryp} + F_{Rys} \\ N_R = x_dY_R + (F_{Rxp} - F_{Rxs}) \cdot C_{RR}, \end{cases} \quad (15)$$

where F_{Rxp}, F_{Rxs}, F_{Ryp}, and F_{Rys} are the rudder forces of the port and starboard rudders along the x_b and y_b axes (see section II-D), x_d is the moment arm of the rudder (as shown in Figure 1), and C_{RR} is the distance from the rudder to the middle line plane. X_P and N_P are the propeller thrust and yaw moment. For a twin-propeller ship, we have

$$\begin{cases} X_P = (1-t_p)[T_p(u) + T_s(u)] \\ Y_P = 0 \\ N_P = (1-t_p)[T_p(u) - T_s(u)] \cdot C_{PP}, \end{cases} \quad (16)$$

where t_p is the thrust deduction factor of the propeller, $T_p(u)$ and $T_s(u)$ are the each propeller thrust of the port and starboard sides (see section II-C), and C_{PP} is the distance from the propeller to the middle line plane. For a single-propeller single-rudder ship, we have $C_{RR} = C_{PP} = 0$. Finally, the cross-flow loads closely linked to vortex shedding are expressed as follows [30]

$$\begin{cases} X_{CF} = 0 \\ Y_{CF} = -0.5\rho \int_L [C_D(x)V_{CF}|V_{CF}|T(x)]\mathrm{d}x \\ N_{CF} = -0.5\rho \int_L [C_D(x)xV_{CF}|V_{CF}|T(x)]\mathrm{d}x, \end{cases} \quad (17)$$

where $C_D(x)$ is the 2D cross-sectional drag coefficient. This is a strip theory approach and $C_D(x)$ can be estimated by using Hoerner's curve [31]. The transverse velocity of the cross-section is $V_{CF} = v + xr$, $T(x)$ is the local draft, and ρ is the water density. Y_{CF} and N_{CF} are nonlinear viscous cross-flow drags at large drift angles. If the surge cross-flow drag X_{CF} and potential damping X_u are included in the total resistance $R_T(u)$, then $X_{CF} = X_u = 0$.

Having a great influence on the ship motions, the viscous damping mainly includes components of skin friction, eddy-making damping, wave drift damping, and damping due to lifting forces of the hull [12], [30]. Generally, it is difficult to separate these effects. In present study, the skin friction, eddy-making damping, wave drift damping (see section II-E), and surge damping (see section II-C) are considered. Results from comparisons between calculations and experimental data show that damping components should be reasonably corrected to improve the accuracy of the motion predictions.

C. RESISTANCE AND PROPULSION MODELS

Conventional vessels are subjected to longitudinal viscous drags including the resistances above and below the waterline when sailing in calm water. The total calm water resistance R_T is expressed as follows [8], [32]

$$R_T = R_F(1+k_1) + R_W + R_A + R_{APP} + R_B + R_{TR}, \quad (18)$$

where R_F is the ITTC1957 frictional resistance, k_1 is the hull form factor considering the viscous pressure resistance, R_W is the wave-making resistance, R_A is the sum of the air resistance without wind and the additional frictional resistance due to the effects of the hull roughness, R_{APP} is the appendage resistance, R_B is the additional pressure resistance due to the bulbous bow near the water surface, and R_{TR} is the additional pressure resistance resulting from transom immersion. These subdivisions are estimated by using the Holtrop-Mennen method [32]. In general, R_{APP} accounts for 3-10% of the total resistance, and is ignored in present study since we could not obtain accurate parameters of appendages.

The propulsion model is based on the Wageningen B-series propeller [33]. The nondimensional thrust coefficient of the single propeller in open water is calculated by using the following formulas

$$K_T = \frac{T}{\rho n^2 D_P^4}, \quad (19)$$

where T is the thrust generated by a single propeller, n is the revolutions of propeller per second, and D_P is the propeller diameter. According to the Reynolds number R_n at the propeller, the thrust coefficient is further expressed as

$$K_T(R_n) = K_T(R_n = 2.0\times10^6) + \Delta K_T(R_n), \quad (20)$$

where $R_n = c_{0.75R}U(1-w_p)[1+(0.75\pi/J)^2]^{0.5}/\nu$, $c_{0.75R}$ is the chord length at $0.75R$ radius of the propeller, U is the ship forward speed, w_p is the wake fraction, J is the advance ratio coefficient, ν is the water kinematic viscosity, and $\Delta K_T(R_n)$ is the corrected value due to the additional Reynolds number effect when $R_n \in (2.0\times10^6, 2.0\times10^9]$. The original open-water test data of $K_T(R_n)$ is given by [33].

D. RUDDER MODEL

The coordinate system O_R-$x_Ry_Rz_R$ and parameters employed to calculate the rudder forces and moments are as shown in Figure 2. The origin O_R is located at the rudder center of gravity and positive z_R points downwards.

For a single all-movable rudder with an aspect ratio $\Lambda < 3$, the hydrodynamic forces and moments acting on the rudder are expressed in the form of lift force L and drag D [8]

$$\begin{cases} F_{Rx} = L\sin(\beta_R) - D\cos(\beta_R) \\ F_{Ry} = -L\cos(\beta_R) - D\sin(\beta_R) \\ F_{Rn} = x_d F_{Ry}, \end{cases} \quad (21)$$

where the lift force on rudder is $L = 0.5C_L\rho A_R(u_{RS}^2 + v_{RS}^2)$, the drag $D = 0.5C_D\rho A_R(u_{RS}^2 + v_{RS}^2)$, and coefficients C_L and C_D are found from the expressions

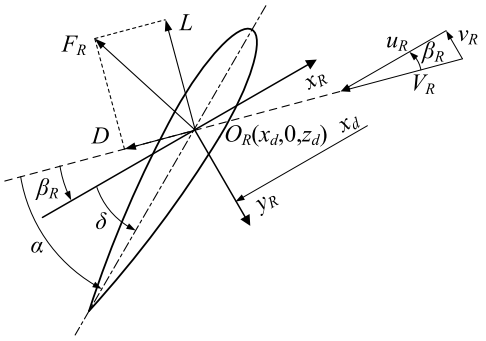

FIGURE 2. Inflow coordinate system of the rudder.

$$\begin{cases} C_L = 2\pi\dfrac{\Lambda(\Lambda+0.7)}{(\Lambda+1.7)^2}sin(\alpha) + C_Q sin(\alpha)\,|sin(\alpha)|\,cos(\alpha) \\ C_D = C_L^2/\pi\Lambda + C_Q\,|sin(\alpha)|^3 + C_{D0}, \end{cases} \quad (22)$$

where longitudinal and transverse components of the mean inflow velocity V_R are $u_{RS} = U(1-w_p)\left[1+k_m\left(\sqrt{1+C_T}-1\right)\right]$ and $v_{RS} = \gamma_v v + \gamma_r x_d r$, respectively, the drift angle of the rudder is $\beta_R = atan(-v_{RS}/u_{RS})$, the effective angle of attack is $\alpha = \delta - \beta_R$, $C_Q \in [0,1]$ is the resistance coefficient, C_{D0} is the rudder surface friction, $k_m \in [0.5, 1]$ is the velocity coefficient, the thrust loading coefficient is expressed as $C_T = 8.0K_T/\pi J^2$, γ_v and γ_r are the flow rectification factors based on experimental data. Note that (22) does not involve the interaction effects among the rudders.

E. MEAN SECOND-ORDER WAVE LOADS

The nonlinear wave loads mainly comprise three components, i.e. nonoscillatory forces - mean second-order wave drift forces, low-frequency second-order slowly-varying drift forces, and high-frequency high-order forces in irregular waves [12], [30]. Being related to the hull's ability to cause waves and the relative vertical motion between the ship and the waves, the mean second-order drift forces can induce the ship to drift or exert a suction force on submersibles near the free-surface. When the ship is moving up and down in water, the average pressure on the varying wetted area of the hull is not zero, resulting in displacement changes. The slowly-varying drift forces (difference frequency loads) can cause large slow drift motions due to the resonance from the nonlinear interaction between the waves and the ship motions when the damping is low. Additionally, the drift motions combine with the first-order linear motions. The high-frequency forces oscillating with sum frequencies can produce oscillation in the structure of the ship, such as "springing" and "ringing." However, the high-frequency forces can be ignored since it does not affect the ship motions. When slowly-varying drift forces are included, the third-order wave drift damping should also be considered.

This paper only considered the influence of mean second-order wave drift forces on ship motions. The 3D boundary element method (BEM) based on Green function source is adopted to solve the velocity potential of the flow field. Some assumptions are made that the fluid is incompressible, nonviscous, and the flow is irrotational. In the seakeeping coordinate system, the total potential is decomposed into

$$\varphi_T = \varphi_B + \varphi_I + \varphi, \tag{23}$$

where $\varphi_B = -Ux$ is the Neumann-Kelvin basis flow potential, φ_I is the incident waves potential, and disturbance potential is $\varphi = \varphi_D + \varphi_R$, which is the sum of the diffraction potential and the radiation potential. Therefore, the far-field potential is $\phi = \varphi_I + \varphi$.

Solving the boundary value problem (BVP) of potential φ_T is to obtain the solution of potential φ, which satisfies the Laplace equation inside the solution domain, the dynamic and kinematic boundary conditions on the free-surface, and the body boundary condition on the hull surface. The radiation condition are also satisfied at infinity of the free-surface and the water depth. Then the integrals over the fluid domain can be transformed into those over the boundaries of the fluid domain by using the Green's second identity. The resulting boundary integral equation expressed by the Green function can be obtained by [7]

$$c(p)\varphi(p) = \iint_S \left[G(p,q)\frac{\partial \varphi(q)}{\partial n} - \varphi(q)\frac{\partial G(p,q)}{\partial n} \right] dS_q, \tag{24}$$

where $p(x, y, z)$ and $q(\xi, \eta, \zeta)$ are the field point and source point, respectively, S is the closed boundary surface of the flow field, which is composed of free surface, body surface and control surface. When p is inside the solution domain, $c(p) = 4\pi$, and $c(p) = 2\pi$ when p is on the smooth surface, n is the unit normal into the ship.$G(p,q)$ is the Green function source that satisfies free surface conditions [23], [30], the far-field asymptotic approximation of the Green function is [24]

$$G(p,q) = 2\pi k i \exp[k(z+\zeta)]H_0^{(1)}(kR) + 0(k^{-1}R^{-2}) + 0(\zeta R^{-2}), \tag{25}$$

where $k = \omega^2/g$ is the wave number in deep water, ω is the wave frequency, i is imaginary unit, $H_0^{(1)}$ is the Bessel function of the third kind (Hankel function), and R is given by $R = [(x-\xi)^2 + (y-\eta)^2]^{1/2}$.

The hull surface is discretized into quadrilateral elements with the Green function source points distributed. The source density over each element is calculated by using the body boundary condition. The velocity potential φ is obtained by solving (24). Experience suggests that the number of elements for the half-hull should usually be 700-1500, and the element size should be less than 1/8-1/10 of the minimum wavelength [30]. According to the Bernoulli equation, the pressure at each point in fluid domain can be obtained from the far-field velocity potential ϕ.

Then substituting (25) into (24), it follows that

$$\varphi(p) = \left(\frac{k}{2\pi R_0}\right)^{1/2} K(\pi+\alpha,\omega)\exp(kz + ikR_0 + \pi i/4) + 0(k^{-1/2}R_0^{-3/2}K), \tag{26}$$

where $R_0 = (x^2+y^2)^{1/2}$, α is the polar angle in cylindrical coordinate system,$K(\alpha,\omega)$ is the Kochin function, related to the far-field potential ϕ, and can be given by

$$K(\alpha,\omega) = \iint_S \left(\frac{\partial \varphi(q)}{\partial n} - \varphi(q)\frac{\partial}{\partial n}\right) \times \exp(k\zeta + ik\xi\cos\alpha + ik\eta\sin\alpha)\, dS_q, \tag{27}$$

Based on the principle of conservation of momentum, the mean second-order wave drift forces acting on the ship can be expressed as

$$\begin{cases} \overline{R_X} = \dfrac{\rho k^2}{8\pi}\displaystyle\int_0^{2\pi} |K(\alpha,\omega)|^2\cos(\alpha)d\alpha \\ \quad + \dfrac{\rho\omega\zeta_a}{2}\cos(\chi)ImK(\pi+\chi,\omega) \\ \overline{R_Y} = \dfrac{\rho k^2}{8\pi}\displaystyle\int_0^{2\pi} |K(\alpha,\omega)|^2\sin(\alpha)d\alpha \\ \quad + \dfrac{\rho\omega\zeta_a}{2}\sin(\chi)ImK(\pi+\chi,\omega) \\ \overline{M_Z} = -\dfrac{\rho k}{8\pi}Im\displaystyle\int_0^{2\pi} K^*(\alpha,\omega)K'(\alpha,\omega)d\alpha \\ \quad - \dfrac{\rho\omega\zeta_a}{2k}ReK'(\pi+\chi,\omega), \end{cases} \tag{28}$$

where ζ_a is the wave amplitude, χ is the encounter wave angle, $|K(\alpha,\omega)|^2 = K(\alpha,\omega)K^*(\alpha,\omega)$, the asterisk denotes the complex conjugate, and $K'(\alpha,\omega) = dK(\alpha,\omega)/d\alpha$.

Real ocean waves are similar to short-crested irregular waves in case of extreme weather. The effect of short-crestedness can be modeled by the directional spectrum [12]

$$S(\omega,\theta) = S(\omega)f(\theta), \tag{29}$$

where $S(\omega)$ is the spectrum of long-crested irregular waves, $f(\theta)$ is the directional spreading function, and θ is the angle between the each wave component and the main wave propagation direction. This paper adopts the modified Pierson-Moskowitz (MPM) spectrum recommended by ITTC to be applied for a fully developed sea with infinite depth, no swell and unlimited fetch

$$S(\omega) = A\omega^{-5}\exp(-B\omega^{-4}), \tag{30}$$

where $A = 4\pi^3 H_s^2/T_z^4$, $B = 16\pi^3/T_z^4$, H_s is the significant wave height, and T_z is the zero-crossing period. The directional spreading function is

$$f(\theta) = \begin{cases} 2\cos^2\theta/\pi, & |\theta| \le \pi/2 \\ 0, & \text{elsewhere}, \end{cases} \tag{31}$$

When the ship is moving at speed U, the encounter frequency can be expressed as $\omega_e = \omega - kU\cos(\chi)$. The wave

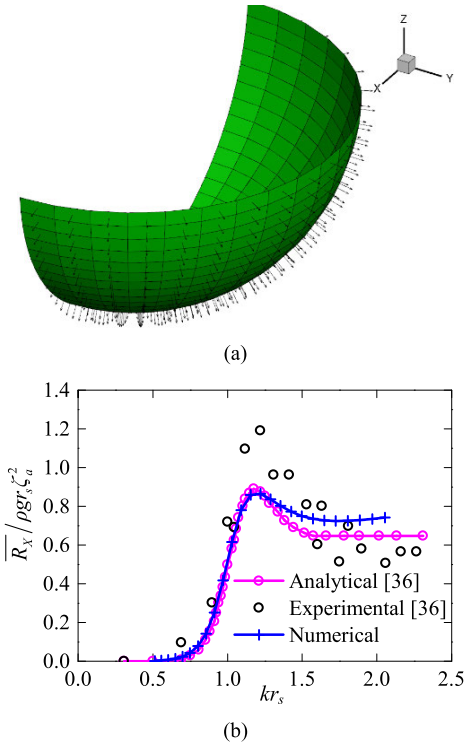

FIGURE 3. The panel model and surge drift force of a freely floating hemisphere with the radius $r_s = 1$ m, wave amplitude $\zeta_a = 1$ m, main wave direction $\beta_a = 0°$ which means the following sea. Fig. 3a (top) shows the panel model. Fig. 3b (bottom) shows the validation of wave drift force acting on the freely floating hemisphere.

elevation $\zeta(t)$ of the short-crested irregular waves in terms of the encounter frequency is given by

$$\zeta(t) = \sum_{i=1}^{N}\sum_{j=1}^{M}\sqrt{2S(\omega_i,\theta_j)\Delta\omega_i\Delta\theta_j}\sin(\omega_{ei}t + \phi_{\zeta ij} + \phi_{pij}), \tag{32}$$

where ω_{ei} is the encounter frequency of the wave component number i, $\phi_{\zeta ij}$ is the random phase angle of the i-th wave component in the j-th direction θ_j, and the position-dependent phase angle is $\phi_{pij} = -k_i x_n \cos(\theta_j) - k_i y_n \sin(\theta_j)$. In the numerical simulations, the number of wave component N and the direction M should be reasonably selected to ensure the generated pseudo-random numbers of the phase angles $\phi_{\zeta ij}$ are uniformly distributed between $[0,2\pi]$.

The numerical calculation of the drift force for a freely floating hemisphere is implemented and verified by applying the above methods in the frequency domain [23], [34]. The discrete elements of the surface of the hemisphere with a radius $r_s = 1$ m are shown in Figure 3a. The comparisons of the nondimensional surge drift force between the numerical result, and Kudou's [36] analytical solution and test data are referred to Figure 3b. In general, the drift loads, as the second order quantities, are small and difficult to be measured in a model test. Thus, the model test results contain uncertainties. The numerical curve has a peak and this tendency is also confirmed by the experimental results. And the numerical result agrees well with the analytical and experimental values in the range of low frequency $kr_s < 1.3$, and is slightly larger at high frequency $kr_s > 1.3$, where the wavelength becomes short. Therefore, the error of the drift force calculated by the present far-field method increased in the high frequency band. In this paper, the calculations of drift forces are conducted mainly in the low frequency band.

TABLE 1. Principal characteristics of NHJ111 and Mariner.

Parameter	Value	
	NHJ111	Mariner
Hull particulars		
Length between perpendiculars L_{pp} (m)	88.0	160.9
Breadth B (m)	15.2	23.2
Draft T (m)	5.6	7.5
Displacement (m^3)	4295.61	16390.24
Block coefficient C_b	0.571	0.610
Centre of gravity COG (x_g, y_g, z_g) (m)	(-0.294, 0.0, 0.706)	(0.0, 0.0, 2.45)
Design ship speed U (knots [a])	19.73	20.0
Propeller revolutions N_{rev} at U (rpm [b])	257.9	92.6
Engine rate of revolution (rpm)	750	—
Propeller particulars		
Type	Controllable pitch	—
Number of propellers	2	1
Number of blades Z	4	4
Diameter D_P (m)	3.8	6.7
Pitch ratio P/D_P	0.74	1.038
Blade area ratio A_E/A_O	—	—
Direction of rotation	Right-handed	Right-handed
Rudder particulars		
Type	Underhung balanced	Semi-balanced
Number of rudders	2	1
Rudder area A_R (m^2)	7.5	25.3
Aspect ratio Λ	1.2	1.89
Maximum rudder angle δ (°)	±35	±(37-40)

[a] 1 knot = 0.5144 m/s.
[b] rpm represents revolutions per minute.

III. NUMERICAL CALCULATIONS AND VERIFICATIONS

In this section, the maneuvering and seakeeping analyses of two ships (NHJ111 and Mariner) are investigated, and the motions and loads are modeled by using previous methods. The principal characteristics of the two ships are given in Table 1, and the calculation conditions are shown in Table 2. To solve the BVP of disturbance potential φ, the number of quadrilateral elements for the two half hulls are 1288 and 1183, respectively, as shown in Figure 4. Equation (5) is employed, in which the drift forces τ_{wave2} are calculated by using (28). The classical fourth-order Runge-Kutta algorithm is utilized to numerically integrate (1) to obtain the responses of the ship motions in the time domain in O_n-$x_n y_n z_n$.

NHJ111 is a twin-propeller twin-rudder ship, whereas the Mariner is a single-propeller single-rudder ship (see Table 1). Therefore, it is necessary to distinguish the calculations of the thrust forces and rudder forces (see the explanation of (15) and (16)). At the equilibrium of resistance $R_T(u)$ and thrust X_P in calm water, the revolutions of propeller are $N_{rev} = 198.4$ rpm and 71.8 rpm for NHJ111 and Marine, respectively, according to the initial forward speeds U_0 (see Table 2). The revolutions remain unchanged during calculations, and the influence of waves on thrust and rudder forces is ignored.

The hydrodynamic coefficients of the added mass and damping in $\boldsymbol{M_A}(\infty)$ and $\boldsymbol{D}(\infty)$ for both ships are obtained

TABLE 2. Calculation conditions and settings.

Parameter	Calm water NHJ111/Mariner	Short-crested irregular waves Mariner
Initial forward speed U_0 (knots)	16.0/15.4	15.4
Propeller revolutions N_{rev} at U_0 (rpm)	198.4/71.8	71.8
Command rudder angle δ_c (°)	35.0/20.9	20.9
Main wave direction β_a (°)	—	150.0
Significant wave height H_s (m)	—	3.0
Zero-crossing period T_z (s)	—	10.0
Wave frequency ω (rad/s)	—	0.1-2.4
Water depth h_{wd} (m)	∞	∞
Calculation time step h_1 (s)	0.1	1.0

TABLE 3. Added mass and damping coefficients of NHJ111 and Mariner at the steady forward speed.

Parameter	NHJ111 hull		Mariner hull		Unit
	Present method	Empirical method	Present method	Empirical method	
$X_{\dot{u}}$	-1.85e+05	-2.77e+05	-7.11e+05	-1.05e+06	kg
$Y_{\dot{v}}$	-4.21e+06	-4.87e+06	-1.50e+07	-1.73e+07	kg
$Y_{\dot{r}}$	-1.47e+07	-3.57e+07	-1.16e+08	-1.50e+08	kg·m/rad
$N_{\dot{v}}$	-1.47e+07	-3.08e+07	-1.16e+08	-0.72e+08	kg·m
$N_{\dot{r}}$	-2.14e+09	-1.81e+09	-2.17e+10	-2.56e+10	kg·m^2/rad
Y_v	-2.64e+04	-3.01e+05	-8.38e+04	-7.89e+05	kg/s
Y_r	-2.08e+04	5.52e+06	-5.34e+04	3.11e+07	kg·m/(s·rad)
N_v	-2.08e+04	-1.07e+07	-5.11e+04	-4.40e+07	kg·m/s
N_r	-2.45e+07	-3.74e+08	-2.32e+08	-3.36e+09	kg·m^2/(s·rad)

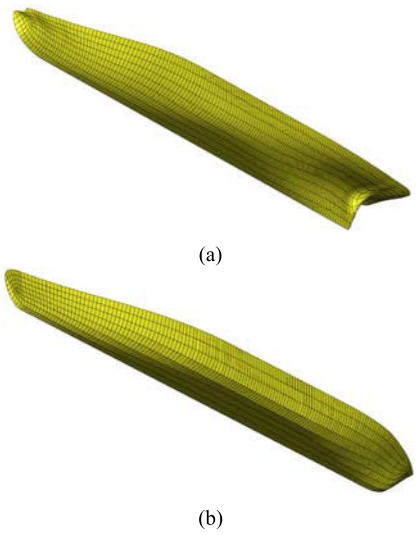

FIGURE 4. The panel models of the half hulls of NHJ111 (Fig. 4a) and Mariner (Fig. 4b).

by two methods. The present 3D BEM based values for these terms are compared with the empirical equation method in Table 3. Liu *et al.* [37] made a literature review of empirical maneuvering models, in which regression formulas of Clarke *et al.* [38] based on large numbers of Planar Motion Mechanism (PMM) tests are used to estimate the coefficients.

A. VERIFICATIONS IN CALM WATER

Parameters for the turning motion of NHJ111 in calm water are shown in Table 1 and Table 2. Figures 5 shows the comparison between BEM based numerical results and empirical equation results. Both methods give almost the same trajectories for the initial part and diverse after the heading changed 180°. The stable turning circles are quite different, which may be the results of the ship geometry (the empirical method can not fully consider it), 3D BEM hydrodynamic properties and the relatively large turning angles. Initially, the ship is located at $(x_n,y_n) = (0,0)$, and there is a slight transverse kick in the earlier stage of the turning maneuver in both situations, see Figure 5b. During the turning motion, the surge speed u gradually decreases from the initial speed 8.23 m/s, reaching the steady value of 4.3 m/s, which has a speed drop of 47.8%, as shown in Figure 6.

Table 4 shows the comparisons between the calculated value, empirical result and experimental data. For numerical results, the advance at heading angle 90° $x_{n,90}$ and the diameter of steady turning circle D_c are quite close to the experimental data, whereas the relative errors of the transfer $y_{n,90}$ at 90° change of heading and the turning time T_{360} changing from 0 to 360° of heading are about 7.0%, relatively larger than those of the former two. For empirical results, the relative errors of D_c and T_{360} are larger, and T_{360} has an error of 18.4%. Consequently, the overall relative error of numerical results is within 8.0%, indicating that the mathematical

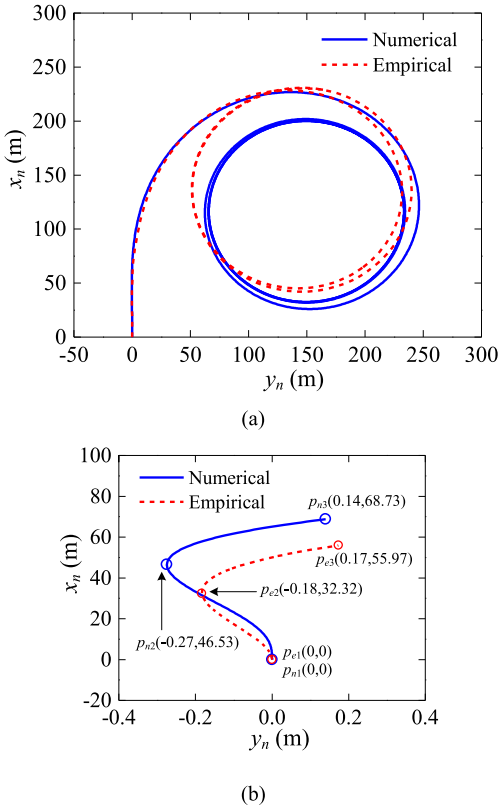

FIGURE 5. Starboard $\delta = 35°$ turning trajectory for NHJ111 at $U_0 =$ 16.0 knots in calm water. Fig. 5a (top) shows the complete turning path based on the BEM method and empirical method, whereas Fig. 5b (bottom) shows the partial path with origin p_{n1}/p_{e1} and point p_{n2}/p_{e2} at maximum transverse kick.

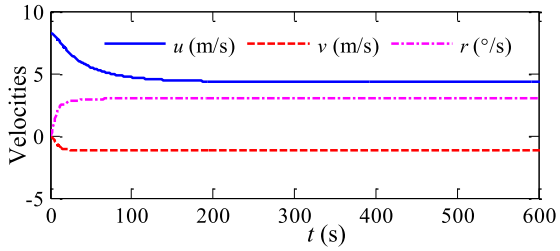

FIGURE 6. Velocities time history of NHJ111 in calm water at $U_0 =$ 16.0 knots, $\delta = 35°$, based on the BEM method.

models and calculation methods can guarantee the precision. According to the analysis in section II-B, the damping terms have dramatic impacts on the motion predictions. The errors may relate to factors such as ignoring the fluid memory effects (see (4)) and influence of the roll motion on horizontal motions, as well as the accuracy of the resistance, propeller and rudder models.

Parameters and calculation conditions of the Mariner are shown in Table 1 and Table 2, and the turning maneuver in calm water are presented in Figure 7 and Figure 8. The numerically calculated trajectory agrees well with the full-scale experimental data [39], and exhibits an improved trajectory prediction compared with the empirical result. Theoretical

TABLE 4. Comparison of NHJ111 turning maneuver between the BEM numerical calculation, empirical method and test in calm water.

Parameter	Test [a]	Numerical calculation		Empirical method	
		result	error	result	error
$x_{n,90}$ (m)	225.6	224.7	0.4%	225.3	0.1%
$y_{n,90}$ (m)	106.2	114.1	7.3%	101.5	4.4%
D_c (m)	169.7	168.9	0.5%	183.1	7.9%
T_{360} (s)	138.0	129.0	6.5%	112.6	18.4%

[a] The test data was provided by Nanhai Rescue Bureau (NRB) of Peoples Republic of China (PRC).

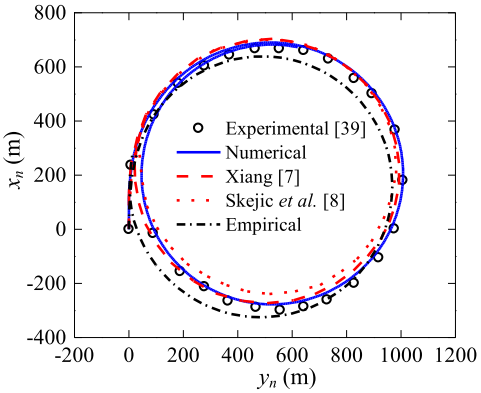

FIGURE 7. Starboard $\delta = 20.9°$ turning trajectory for Mariner at $U_0 =$ 15.4 knots in calm water.

results of Xiang [7] and Skejic *et al.* [8] are also presented in Figure 7, which used the 2D strip theory and the 3D Rankine source method, respectively. As shown in Figure 7, the results of the 3D methods are closer to the trial data than those of the 2D approach. Figure 8 shows the comparisons of the velocities u, v, and r between the calculated results and theoretical results of Skejic et al. [8]. The velocity u decreases with time in both cases. When the turning motion becomes stable, u is slightly larger and v is smaller than the results of Skejic et al., and the r curves of the two cases are coincident. These differences lead to the trajectory results displayed in Figure 7 that the calculated values are closer to the trial data.

B. VERIFICATION OF MARINER IN IRREGULAR WAVES

The loads and motion responses of the Mariner in short-crested irregular waves are numerically calculated and validated by using the BEM method in this section. Based on $T_z =$ 10.0 s of the calculation conditions in Table 2, the corresponding wavelength is $\lambda \approx 156.1$ m. In the case of the nondimensional incident wavelength $\lambda/L_{pp} \approx 1.0$ and $C_b < 0.75$ which means the hull is the slender type, the drift forces could be evaluated by using the above far-field method [7], [8]. The wave frequency is taken as 0.1-2.4 rad/s, covering as much of the response range of ship motions as possible, and only mean second-order wave drift forces of environmental disturbance loads are involved. Regarding the calculations of the mean drift forces, most previous studies dealt with ship maneuvering in regular waves. Therefore, comparisons of the results between this study and others in regular waves

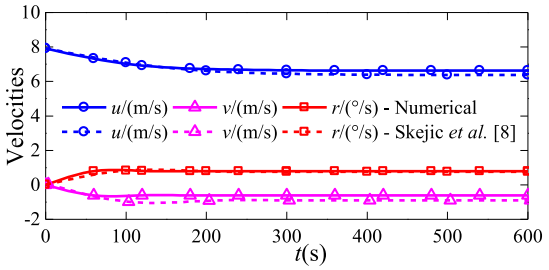

FIGURE 8. Velocities time history of Mariner in calm water at U_0 = 15.4 knots, $\delta = 20.9°$.

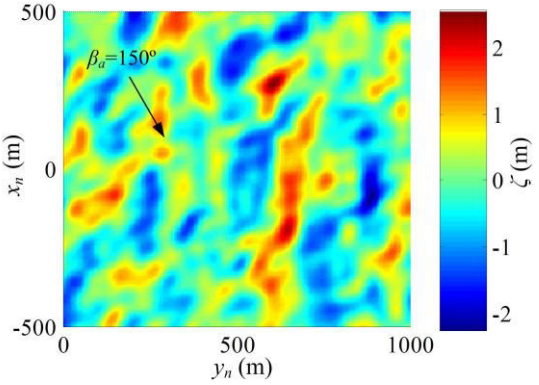

FIGURE 9. Numerical simulation of the 3D spatial field of wave elevation ζ at a certain time with $H_s = 3.0$ m, $T_z = 10.0$ s, $\beta_a = 150°$.

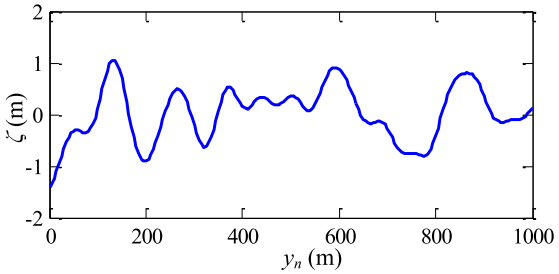

FIGURE 10. 2D wave elevation ζ at cross section of $x_n = -500$ m.

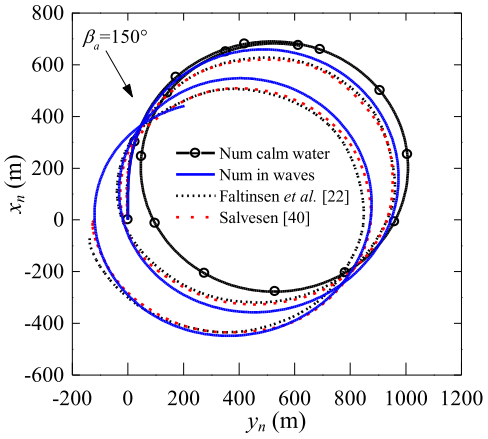

FIGURE 11. Turning trajectory of Mariner in short-crested irregular waves with U_0 = 15.4 knots, $\delta = 20.9°$, $H_s = 3.0$ m, $T_z = 10.0$ s, $\beta_a = 150°$.

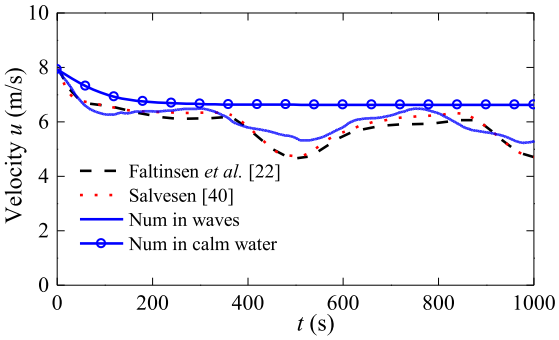

FIGURE 12. Velocity time history of Mariner in short-crested irregular waves with U_0 = 15.4 knots, $\delta = 20.9°$, $H_s = 3.0$ m, $T_z = 10.0$ s, $\beta_a = 150°$.

are performed to verify the methods presented in this paper. The available numerical data employed for comparisons are mainly from Skejic *et al.* [8], Faltinsen *et al.* [22], and Salvesen [40], in which the amplitude of the regular waves is $\zeta_a = 1.5$ m in calculations of the mean drift forces for the Mariner. Consequently, the significant wave height of the irregular waves is taken as $H_s = 3.0$ m, as shown in Table 2.

The 3D contour map of the wave elevation ζ generated by using the MPM spectrum in the field of 1000 m × 1000 m at a certain time is shown in Figure 9. The 2D wave elevation at $x_n = -500$ m is shown in Figure 10.

Figure 11 and Figure 12 show the results of the turning trajectory and surge speed u. The ship is initially located at $(x_n, y_n) = (0,0)$. The numerically calculated trajectory in waves is consistent with the theoretical results of Faltinsen and Løken [22] and Salvesen [40]. Compared with the turning trajectory in calm water, the mean second-order wave forces induce a drift motion with the drift distance about 150.0 m. The drifting of the ship is not in the direction of the incident waves, which is primarily due to the yaw moment $\overline{M_Z}$ that has an importance on ship path predictions [8]. The ship speed u agrees with the theoretical solutions of Faltinsen *et al.* and Salvesen. There is also a speed reduction during the turn maneuver. However, the speed u changes periodically with the drift forces and is smaller than that in calm water under the action of the surge force $\overline{R_X}$, which is also known as the added resistance.

Figure 13 shows the numerical and theoretical results of the nondimensional drift forces and moment as a function of the encounter wave angle χ. The calculated results for short-crested irregular waves in this paper are basically consistent with the theoretical solutions in regular waves by other researchers [22], [40]. When the encounter angle $\chi = 0°$ which means the following sea, the added resistance $\overline{R_X}$ is the smallest, and the largest when $\chi = -180°$. When $\chi = 0°$ or $-180°$, the lateral force $\overline{R_Y}$ is close to zero; when $\chi = 90°$ or $-90°$ (beam waves), it reaches the maximum value. In the case of following sea, head sea, and beam sea, the yaw moment $\overline{M_Z}$ is the smallest; it reaches the maximum value when the ship undergoes the bow sea or quartering sea. Because of the stochastic characteristics of short-crested

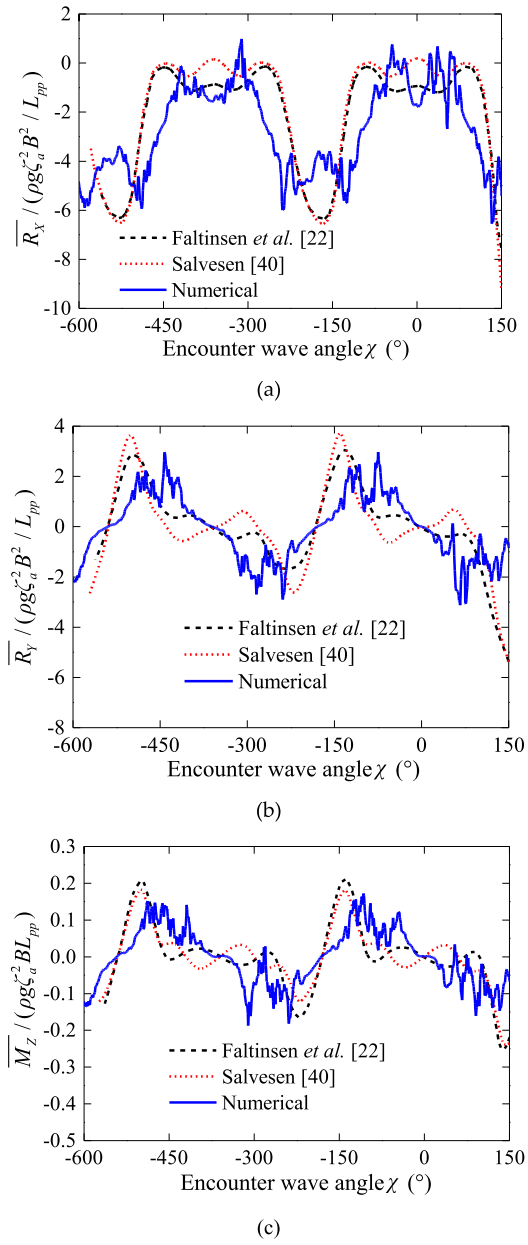

FIGURE 13. Nondimensional drift forces and moment of Mariner against encounter wave angle χ in short-crested irregular waves with $U_0 = 15.4$ knots, $\delta = 20.9°$, $H_S = 3.0$ m, $T_Z = 10.0$ s, $\beta_\sigma = 150°$. Fig. 13a (top), Fig. 13b (middle), and Fig. 13c (bottom) are the added resistance, the mean second-order sway force, and the mean second-order yaw moment, respectively.

irregular waves, calculated drift forces and moment oscillate significantly, especially in the range of peaks and troughs.

The relations between the added resistance $\overline{R_X}$ and speed u are analyzed from Figures 12 and 13 as well. The ship speed u gradually decreases under the action of the added resistance $\overline{R_X}$ when it reaches the maximum in the head sea. It reaches the maximum trough three times, and the speed u also reaches the minimum value three times, as shown in Figure 12 and Figure 13a. The amplitudes of the calculated drift forces and moment are slightly smaller than those of

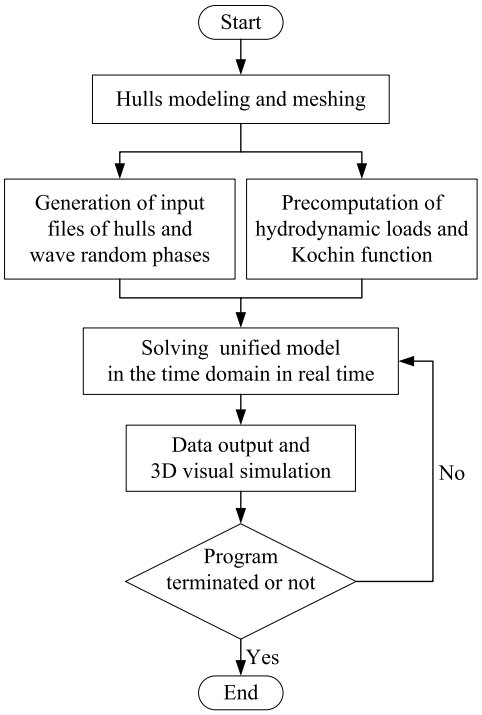

FIGURE 14. Flow chart for real-time calculations of ship motions.

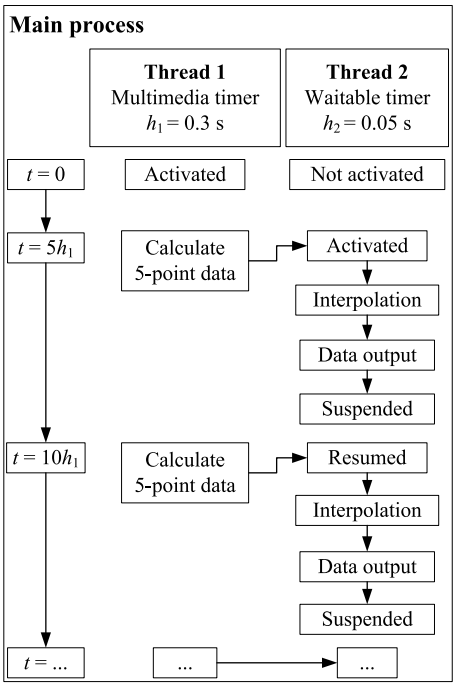

FIGURE 15. Schematic diagram for the real-time calculation method of solving the unified model in the time domain.

Faltinsen and Løken [22] and Salvesen [40], especially at the peak and trough. As a result, the calculated speed u is slightly larger. During calculations, wave components with different random phases can affect the ship trajectory and drift forces. It is necessary to ensure that the generated random phases are uniformly distributed over $[0, 2\pi]$.

Main process:

```
line 1:   int token_go=0;          //0, Interpolation is allowed for waitable timer; 2, Not allowed.
line 2:   int token_usevars=1;     //1, Storing 5-point data in Y1; 2, Storing 5-point data in Y2.
line 3:   matrixd Y1(5,1);         //Used to store 5-point data, depending on variable token_usevars.
line 4:   matrixd Y2(5,1);
line 5:
line 6:   Thread 1: multimedia timer, h1 = 0.3 s
line 7:   {
line 8:      Solving equations of (1) and (5);
line 9:      if (1 == token_usevars)  {Y1 = values of 5-point data;  token_go = 1;  token_usevars = 2;}
line 10:     if (2 == token_usevars)  {Y2 = values of 5-point data;  token_go = 1;  token_usevars = 1;}
line 11:  }
line 12:
line 13:  Thread 2: waitable timer, h2 = 0.05 s
line 14:  {
line 15:     if (1 == token_go)
line 16:     {
line 17:        if (2 == token_usevars)  {Perform interpolations using Y1; token_go=0;}
line 18:        if (1 == token_usevars)  {Perform interpolations using Y2; token_go=0;}
line 19:        Output the results of interpolations;
line 20:     }
line 21:  }
```

FIGURE 16. Pseudo code of the main program for the real-time calculation method.

According to the comparative analyses, the precision of the numerical results of maneuvering quantities and wave loads in short-crested irregular waves is basically good. The presented mathematical models can be applied to the rescue ship simulator to analyze the maneuvering and seakeeping problems of the ship.

IV. REAL-TIME CALCULATION OF NHJ111 MOTION

The short-crested irregular waves are composed of a series of wave components with multiple frequencies and different spreading directions. Therefore, the computations of wave loads is more time-consuming than those in regular waves. In order to achieve the goal of real-time calculations with high-precision mathematical models, the above-mentioned models are employed together with the high-performance computer hardwares (where high-performance refers to multiple cores, high CPU frequency, and large memory). The adopted PC configurations in the calculations are shown in Table 5. In addition, the method of two-thread double-timer parallel computation combined with the interpolation calculations is conceived in this section. Real-time calculations and 3D visual simulations of the NHJ111 motion are conducted with the verified models in the test platform Virtools, which is a modular software and quite convenient to test ideas.

A. REAL-TIME ALGORITHM DESIGNING

In this section, the development of the real-time algorithm is conducted to implement the above-validated mathematical models in present study. The further development of Virtools is carried out by using the Microsoft Foundation Class Library (MFC) in Microsoft Visual Studio. The general calculation process of the ship motions is shown in Figure 14.

TABLE 5. PC configurations for real-time calculations.

Parameter	Value
Operating system	Windows 7 64-bit
Processor	Intel quad core i5-4460 CPU @3.2GHz
Memory	8.0GB RAM
Graphics card	NVIDIA GeForce GTX750 Ti
Graphic memory	4.0GB
Graphics interface API	DirectX 11

The realization of the real-time algorithm, which we call two-thread double-timer interpolation and synchronization methods, involves two threads in the main process. High-precision timers, namely, the multimedia timer and waitable timer in each thread, are accessed to perform time loop control. Generally, the multimedia timer is used for playback control of computer media, such as video and audio, whereas the waitable timer is used for scheduled tasks on Windows. Once created, both timers run on two independent threads that do not block each other. Their resolutions are in 1 millisecond (ms), which meet the requirement of real-time calculations. The concept of this algorithm is shown in Figure 15, related to the part of solving the unified model in the time domain, as shown in Figure 14.

As shown in Figure 15, thread 2 is not activated in the beginning, and thread 1 is executed five times with a calculation step of h_1, resulting in five data points. Then thread 2 executes interpolation operations of the five-point data with an interpolation step of h_2, and outputs the results. Therefore,

TABLE 6. Real-time calculation conditions of NHJ111 motions.

Parameter	Value
Initial forward speed U_0 (knots)	16.0
Propeller revolutions N_{rev} at U_0 (rpm)	198.4
Command rudder angle δ_c (°)	35.0
Main wave direction β_a (°)	90.0
Significant wave height H_s (m)	5.0
Zero-crossing period T_z (s)	6.25
Wave frequency ω (rad/s)	0.1-2.4
Water depth h_{wd} (m)	∞
Calculation time step h_1 (s)	0.3
Interpolation time step h_2 (s)	0.05

thread 2 is always lagging by $5h_1$ compared with thread 1. In order to achieve the goal of real-time calculations, h_1 must be greater than the actual calculation time needed for one step in addition to ensuring the convergence and stability of the computations of the ship motions.

Figure 16 shows the pseudo code of the main program corresponding to the concept of the algorithm in Figure 15. In the MFC programming for real-time simulations, the c++ template library is used to conduct mathematical modeling and real (complex) matrix operations [41]. Four global variables, namely, *token_go*, *token_usevars*, $Y1$, and $Y2$, are defined. The $Y1$ and $Y2$ store the positions and attitudes for the five-point data in the global coordinate system O_n-$x_ny_nz_n$. The *token_usevars* is used to determine whether the multimedia timer of thread 1 assigns the five- point data to $Y1$ or $Y2$, which is used by the waitable timer of thread 2 for interpolation calculations. The *token_go* is the sign to decide whether the waitable timer performs interpolations or not in order to achieve parallel computing among the two timers. The interpolation method of the Akima cubic polynomials are adopted. The codes of the entire calculation process of the ship motions is encapsulated in a dynamic-link library (DLL), which can be called by other visualization softwares such as Unity3D, VegaPrime or OpenSceneGraph (OSG).

B. REAL-TIME MOTION OF NHJ111 IN WAVES

In this section, real-time calculations and visual simulations of the motions of NHJ111 subjected to the drift forces in short-crested irregular waves are conducted. The main parameters of the ship are shown in Table 1. The employed maneuvering parameters and calculation conditions are shown in Table 6. According to the wavelength $\lambda \approx 60.0$ m in coastal waters of China where the rescue ship NHJ111 is often deployed, the corresponding zero-crossing period is taken as $T_z = 6.25$ s. In the case of the nondimensional incident wavelength $\lambda/L_{pp} \approx 0.68 > 0.5$ and $C_b < 0.75$ which means the hull is the slender type, the above far-field method can be used to calculate the drift forces [7], [8]. The significant wave height is $H_s = 5.0$ m, corresponding to the sea state 6, and the wave elevation ζ generated by using the existing MPM spectrum is similar to that in Figure 9. Wave conditions in this sea area in rough weather can be measured by wave height meters or an x-band radar [42], which has not been carried out yet in this study. The frame rate is 20 Frames Per Second (FPS) based on the interpolation step $h_2 = 0.05$ s, which is greater than the minimum of 15 FPS for real-time visualization.

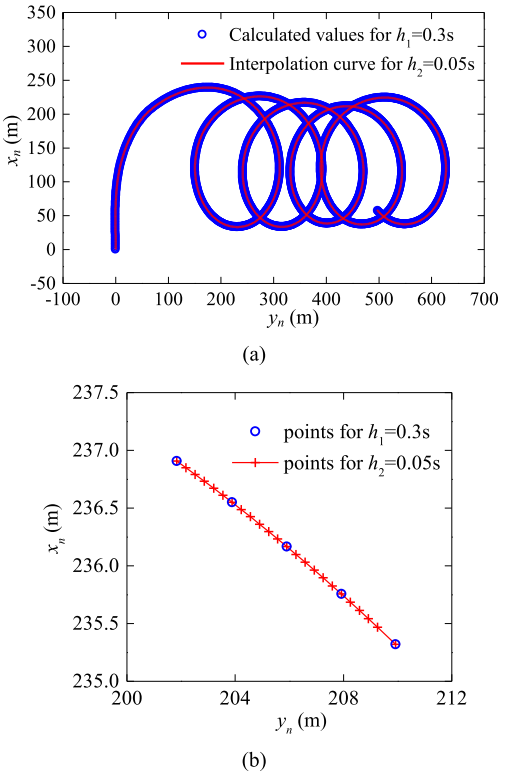

FIGURE 17. Turning trajectory and interpolation results of NHJ111 in short-crested irregular waves with $U_0 = 16.0$ knots, $\delta = 35°$, $H_s = 5.0$ m, $T_z = 6.25$ s, $\beta_a = 90°$. Fig. 17a (top) shows the complete turning trajectory and its interpolation curve. Fig. 17b (bottom) shows the partial turning trajectory for five calculated points and its interpolation points.

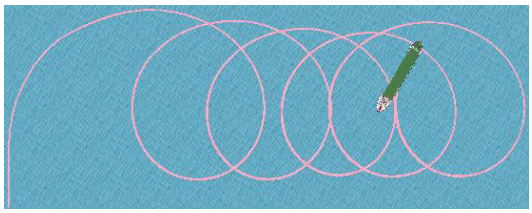

FIGURE 18. The 3D visualization of the NHJ111 motion.

The motion equation is based on (5), and the drift forces are calculated by (28). Equation (1) is numerically integrated by using the fourth-order Runge-Kutta algorithm to obtain the motion responses of $h_1 = 0.3$ s in O_n-$x_ny_nz_n$. The real-time output results of the motion states for $h_2 = 0.05$ s, as shown in Figure 17, are acquired by using the real-time algorithm described in section IV-A. In Figure 17, the starting location is at $(x_n,y_n) = (0,0)$, "o" is the calculation results of $h_1 = 0.3$ s, and "——" as well as "—+—" represents the five-point cubic interpolation results of $h_2 = 0.05$ s. The propeller revolution rate is a constant of 198.4 rpm during the calculation.

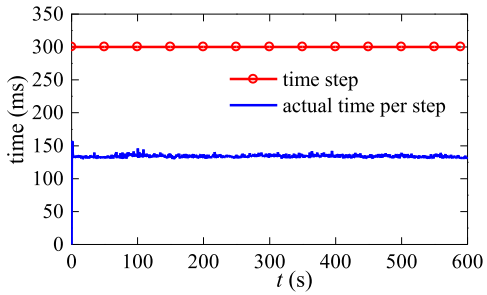

FIGURE 19. The actual calculation time of each step.

The 3D visual simulation of the ship motion is shown in Figure 18, corresponding to Figure 17a. Figure 19 shows the actual time needed at each step $h_1 = 0.3$ s. It can be seen that the average time for calculating one step is about 130 ms, which is less than the specified calculation time step of 0.3 s and greater than the interpolation time step of 0.05 s, and thus satisfy the requirement of real-time calculations. Here we should note that the value of h_1 should be treated carefully due to the truncation error of the fourth-order

Runge-Kutta method is an equivalent infinitesimal of $O(h_1^5)$.

V. CONCLUSION

A combined maneuvering and seakeeping model applied to the rescue ship simulator is established with the aim of achieving high-precision motion predictions and real-time calculations.

Numerical calculations of the turning motions of NHJ111 and Mariner in calm water are conducted. Compared with the experimental data, the relative errors of the calculated results are approximately 7.0%, which indicates the mathematical model has a good precision. The calculated trajectory exhibits an improvement when compared with the empirical result. *Meanwhile*, the turning motions and wave loads of Mariner in short-crested irregular waves are *reported*. The far-field method with fast convergence rate based on the Kochin function is used to calculate the mean drift forces. Compared with the theoretical solutions in regular waves, the calculated trajectory and surge speed u give satisfactory predictions. The calculated drift forces are consistent with the theoretical solutions in general, and slightly smaller at local peaks and troughs where exhibit some stochastic oscillation characteristics. The correlation between the drift forces and the encounter wave angle is analyzed, and the influences of the drift forces on the turning circle and speed u are also elaborated.

According to these comparative analyses, the established mathematical model is able to analyze the maneuvering and seakeeping problems with a good precision. The *method* of two-thread double-timer synchronous interpolations is proposed, and makes it possible to predict ship motions in real time with the present mathematical model. The real-time motion simulation of the rescue ship NHJ111 subjected to the drift forces is thus conducted in short-crested irregular waves.

The presented methods can effectively and instructively predict the ship motions in real time in rough sea, and be applied to the rescue ship simulator which contains multiple ships. In the future, the model of oscillatory motions induced by the first-order wave loads will be developed to extend the current model to 6DOF, and the model of anti-roll u-tank will be added to make it powerful to analyze the ship motions.

REFERENCES

[1] Z. W. Wang, "Current development of rescue and salvage equipments," *J. Mech. Eng. China*, vol. 49, no. 20, pp. 91–100, Oct. 2013.
[2] W. Xiong, *Rescue Engineering*. Dalian, China: Dalian Maritime Univ. Press, 2012.
[3] H. K. Yoon, N. S. Son, and G. J. Lee, "Estimation of the roll hydrodynamic moment model of a ship by using the system identification method and the free running model test," *IEEE J. Ocean. Eng.*, vol. 32, no. 4, pp. 798–806, Oct. 2007.
[4] N. Wang, M. J. Er, and M. Han, "Large tanker motion model identification using generalized ellipsoidal basis function-based fuzzy neural networks," *IEEE Trans. Cybern.*, vol. 45, no. 12, pp. 2732–2743, Dec. 2015.
[5] B. Mei, L. Sun, and G. Shi, "White-black-box hybrid model identification based on RM-RF for ship maneuvering," *IEEE Access*, vol. 7, pp. 57691–57705, 2019.
[6] R. M. Tello, M. Candries, M. Vantorre, G. Delefortrie, D. Peeters, and F. Mostaert, "Ship manoeuvring in waves: A literature review. Version 2_0," Flanders Hydraul. Res. Ghent Univ., Antwerp, Belgium, WL Rapporten 00_096, 2012.
[7] X. Xiang, "Maneuvering of two interacting ships in waves," Ph.D. dissertation, Dept. Mar. Technol., Norwegian Univ. Sci. Technol., Trondheim, Norway, 2012.
[8] R. Skejic and O. M. Faltinsen, "A unified seakeeping and maneuvering analysis of ships in regular waves," *J. Mar. Sci. Technol.*, vol. 13, no. 4, pp. 371–394, Nov. 2008.
[9] R. Skejic and O. M. Faltinsen, "Maneuvering behavior of ships in irregular waves," in *Proc. Int. Conf. Ocean, Offshore Arctic Eng. (OMAE)*, Nantes, France, Jun. 2013, pp. 1–14.
[10] W. E. Cummins, "The impulse response function and ship motions," *Schiffstechnik*, vol. 9, no. 47, pp. 101–109, Jan. 1962.
[11] P. A. Bailey, "Manoeuvring of a ship in a seaway," Ph.D. dissertation, Sch. Eng. Sci., Ship Sci., Univ. Southampton, Southampton, U.K., 1999.
[12] T. I. Fossen, *Handbook of Marine Craft Hydrodynamics and Motion Control*. Hoboken, NJ, USA: Wiley, 2011.
[13] X. K. Zhang, X. J. Chen, Y. Lu, and Y. Yin, "Mathematical model of target ships in maritime simulator," *Shipbuilding China*, vol. 55, no. 3, pp. 125–130, 2014.
[14] X. F. Zhang, "Research on six degrees of freedom mathematical model of ships in maritime simulator," Ph.D. dissertation, Navi. College, Dalian Maritime Univ., Dalian, China, 2009.
[15] X. Zhang, Z. Lyu, Y. Yin, and Y. C. Jin, "Mathematical model of small water-plane area twin-hull and application in marine simulator," *J. Mar. Sci. Appl.*, vol. 12, no. 3, pp. 286–292, Sep. 2013.
[16] X. B. Qian, Y. Yin, X. F. Zhang, and Y. Li, "Influence of irregular disturbance of sea wave on ship motion," *J. Traff. Transp. Eng. China*, vol. 16, no. 3, pp. 116–124, Jun. 2016.
[17] M. C. Fang, K. W. Lin, and Z. H. Shu, "An indigenous PC-based ship simulator incorporating the hydrodynamic numerical model and virtual reality technique," *J. Taiwan Soc. Nav. Archit. Mar. Engrs.*, vol. 23, no. 2, pp. 87–95, May 2004.
[18] S. K. Ueng, D. Lin, and C.-H. Liu, "A ship motion simulation system," *Virtual Reality*, vol. 12, no. 1, pp. 65–76, Mar. 2008.
[19] S. Damitha, K. Nihal, K. Chamath, and R. Rexy, "A six degrees of freedom ship simulation system for maritime education," *Int. J. Adv. ICT Emerg. Regions*, vol. 3, no. 2, pp. 34–47, Mar. 2010.
[20] X. Chen, G. Wang, Y. Zhu, and G. S. Owen, "Real-time simulation of ship motions in waves," in *Proc. Int. Symp. Vis. Comput.*, vol. 7431, Jul. 2012, pp. 71–80.
[21] J. A. Pinkster and K. Bhawsinka, "A real-time simulation technique for ship-ship and ship-port interactions," in *Proc. 28th Int. Workshop Water Waves Floating Bodies (IWWWFB)*, L'Isle-sur-la-Sorgue, France, Apr. 2013, pp. 169–172.
[22] O. M. Faltinsen and A. E. Løken, "Slow drift oscillations of a ship in irregular waves," *Appl. Ocean Res.*, vol. 1, no. 1, pp. 21–31, Jan. 1980.

[23] X. B. Chen, "Hydrodynamics in offshore and naval applications—Part I," in *Proc. Keynote Lecture Conf. 6th Int. Conf. Hydrodynamics*, Perth, WA, Australia, Nov. 2004.
[24] J. N. Newman, "The drift force and moment on ships in waves," *J. Ship Res.*, vol. 11, no. 1, pp. 51–60, Jan. 1967.
[25] W. Zhang, Z.-J. Zou, and D.-H. Deng, "A study on prediction of ship maneuvering in regular waves," *Ocean Eng.*, vol. 137, pp. 367–381, Jun. 2017.
[26] H. Yasukawa and Y. Nakayama, "6-DOF motion simulations of a turning ship in regular waves," in *Proc Int. Conf. Mar. Simul. Ship Manoeuvrability (MARSIM)*, Panama City, Panama, Aug. 2009, pp. M-3/1–M-3/10.
[27] M.-G. Seo and Y. Kim, "Numerical analysis on ship maneuvering coupled with ship motion in waves," *Ocean Eng.*, vol. 38, nos. 17–18, pp. 1934–1945, Dec. 2011.
[28] J. H. Lee and Y. Kim, "Prediction of ship operation performance in waves by seakeeping-maneuvering coupled analysis," in *Proc. 33rd Int. Workshop Water Waves Floating Bodies (IWWWFB)*, Guidel-Plages, France, 2018, pp. 105–108.
[29] G. Chillcce and O. Moctar, "A numerical method for manoeuvring simulation in regular waves," *Ocean Eng.*, vol. 170, pp. 434–444, Dec. 2018.
[30] O. M. Faltinsen, *Sea Loads on Ships and Offshore Structures*. Cambridge, UK: Cambridge Univ. Press, 1990.
[31] S. F. Hoerner, *Fluid Dynamic Drag*. Bakersfield, CA, USA: Hoerner Fluid Dynamics, 1965.
[32] J. Holtrop and G. G. Mennen, "An approximate power prediction method," *Int. Shipbuild. Prog.*, vol. 29, no. 335, pp. 166–170, 1982.
[33] M. W. C. Oosterveld and P. Van Oossanen, "Further computer-analyzed data of the Wageningen B-screw series," *Int. Shipbuild. Prog.*, vol. 22, no. 251, pp. 251–262, Jul. 1975.
[34] M. Philippe, A. Combourieu, C. Peyrard, F. Robaux, G. Delhommeau, and A. Babarit, "Introducing second order low frequency loads in the open-source boundary element method code Nemoh," in *Proc. 11th Eur. Wave Tidal Energy Conf. (EWTEC)*, Nantes, France, Sep. 2015, Art. no. 01198807.
[35] N. E. Kochin, *Theoretical Hydromechanics*. Hoboken, NJ, USA: Wiley, 1964.
[36] K. Kudou, "The drifting force acting on a three-dimensional body in waves," *J. Soc. Nav. Archit. Jpn.*, vol. 1977, no. 141, pp. 71–77, 1977.
[37] J. Liu, R. Hekkenberg, F. Quadvlieg, H. Hopman, and B. Zhao, "An integrated empirical manoeuvring model for inland vessels," *Ocean Eng.*, vol. 137, pp. 287–308, Jun. 2017.
[38] D. Clarke, P. Gedling, and G. Hine, "The application of manoeuvring criteria in hull design using linear theory," *Trans. R. Inst. Nav. Archit.*, vol. 125, pp. 45–68, Mar. 1983.
[39] V. Ankudinov, "Assessment and principal structure of the modular mathematical model for ship maneuverability prediction and real-time maneuvering simulations," in *Proc. Int. Conf. Mar. Simulation Ship Manoeuvrability (MARSIM)*, St. John's, NL, Canada, 1993, pp. 661–662.
[40] N. Salvesen, "Second-order steady-state forces and moments on surface ships in oblique regular waves," in *Proc. Int. Symp. Dyn Marine Vehicles Struct. Waves*, London, U.K., 1974, pp. 225–241.
[41] Eigen. *A C++ Linear Algebra Library*. Accessed: Dec. 11, 2018. [Online]. Available: http://eigen.tuxfamily.org
[42] Y. J. Yang and S. H. Kwon, "Prediction for irregular ocean wave and floating body motion by regularization: Part 1. Irregular wave prediction," *Trans. FAMENA*, vol. 40, no. 4, pp. 41–54, 2016.

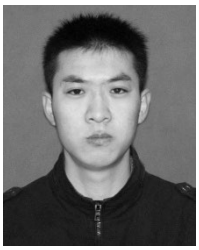

XIAOLEI ZHANG received the B.Sc. and M.Sc. degrees in mechanical engineering from Dalian Maritime University, Dalian, China, in 2010 and 2012, respectively, where he is currently pursuing the Ph.D. degree with Naval Architecture and Ocean Engineering College. His research interests include marine hydrodynamics, visual simulations, and Stewart platform control.

WEI XIONG received the Ph.D. degree in mechanical engineering from the Harbin Institute of Technology, China, in 2001. He is currently a Professor with Naval Architecture and Ocean Engineering College, Dalian Maritime University, Dalian, China. His research interests include fluid transmission and control, virtual assembly, and marine rescue and salvage.

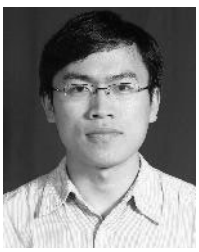

XU XIANG received the Ph.D. degree in marine hydrodynamics from the Norwegian University of Science and Technology (NTNU), Trondheim, Norway, in 2012. He is currently a senior hydrodynamic specialist with Fjordcrossing Department, Norwegian Public Roads Administration. He co-supervises Ph.D. students and serves as an External Examiner for the Department of Marine Technology, NTNU. He is also a Guest Professor with Harbin Engineering University. He is a member of the American Society of Mechanical Engineers.

ZUWEN WANG received the Ph.D. degree in mechanical engineering from Sophia University, Japan, in 1990. He is currently a Professor with Naval Architecture and Ocean Engineering College, Dalian Maritime University, Dalian, China. He is also an Honorary Chairman of the Fluid Transmission and Control Branch and the Chinese Mechanical Engineering Society. His research interests include fluid transmission and control, virtual assembly, and marine rescue and salvage.